Chaos, Solitons and Fractals 142 (2021) 110395

Contents lists available at ScienceDirect

Chaos, Solitons and Fractals

Nonlinear Science, and Nonequilibrium and Complex Phenomena

journal homepage: www.elsevier.com/locate/chaos

Bursting synchronization in neuronal assemblies of scale-free networks

Adriane S. Reis[a], Kelly C. Iarosz[b,c,d], Fabiano A.S. Ferrari[e], Iberê L. Caldas[b], Antonio M. Batista[b,f], Ricardo L. Viana[a,*]

[a] Physics Department, Federal University of Paraná, Curitiba, PR, Brazil
[b] Physics Institute, University of São Paulo, São Paulo, SP, Brazil
[c] Faculdade de Telêmaco Borba, FATEB, Telêmaco Borba, 84266-010, PR, Brazil
[d] Graduate Program in Chemical Engineering Federal Technological University of Paraná, Ponta Grossa, Paraná, 84016-210, Brazil
[e] Institute of Engineering, Science and Technology, Federal University of the Valleys of Jequitinhonha and Mucuri, Janaúba, MG, Brazil
[f] Department of Mathematics and Statistics, State University of Ponta Grossa, Ponta Grossa, PR, Brazil

ARTICLE INFO

Article history:
Received 22 April 2020
Revised 8 October 2020
Accepted 26 October 2020
Available online 3 November 2020

Keywords:
Neuronal network
Scale-free
Synchronization
Suppression

ABSTRACT

We investigate the synchronization properties of a neuronal network model inspired on the connection architecture of the human cerebral cortex. The neuronal model is composed of an assembly of networks, where each one of them is a scale-free network and the connections between them are taken from a human connectivity matrix proposed by Lo and collaborators [J. Neuroscience **30**, 16876 (2010)]. The neuronal dynamics is governed by the Rulkov two-dimensional discrete-time map and the coupling between neurons and the different cortical regions occurs by means of chemical synapses. Individual neurons display bursting activity with characteristic phases and frequencies. Bursting synchronization is achieved for certain values of the chemical coupling strength in the network model and can be related to the presence of some pathological rhythms. The total or partial suppression of bursting synchronization has been pointed as a dynamical mechanism underlying deep brain stimulation techniques to mitigate such pathologies. In this work a synchronization suppression technique is employed through the application of an external signal based on the time-delayed mean field in certain areas of the neuronal network. Our results show that the suppression of synchronization depends on the values of the time delay and intensity of the applied signal.

1. Introduction

The human brain consists of *circa* 10^{11} neurons, linked by $\sim 10^{15}$ connections, which corresponds to an average value of 10^4 synapses per neuron [1]. While we are far from a detailed knowledge of the connection architecture of the brain, there are many neuroanatomic evidences that neurons with similar features are grouped into clusters of 10^5 to 10^6 spatially localized cells [2,3]. Moreover, functional investigations use neuroimaging methods which reveal not only such clustering but also a hierarchical structure, i.e. neuronal clusters form larger clusters and so on, with different levels of description [4–6]. The human brain is one of the natural systems for which the term "complex network" is the most appropriately used, since there is a large number of nodes, connected by a myriad of synapses, and the whole structure exhibits hierarchical features.

Complex networks have been increasingly studied due to their applicability in many research fields like physics, biology and social science [7,8]. These networks can help to detect socials relations [9,10], understand communities behavior and describe physical or mathematical systems [11]. A network is represented by a set of nodes linked to each other by edges [12]. There are many different types of networks of neuroscientific interest, as random (Erdös-Renyi) [13,14], small-world (Watts-Strogatz) [15], and scale-free (Barabasi-Albert) networks [16]. Small-world networks have been identified in many animal and human connectomes [17,18]. In particular, small-world properties have been observed in human brains affected by Alzheimer's disease [19].

Scale-free networks were first reported by Barabási and Albert with the intention of mapping the internet [16]. This type of network can be found in some biological systems, social networks, and also in neuronal assemblies [8,20]. In scale-free networks the number of connections per neuron satisfies a power-law probability distribution, so that highly connected neurons are connected, on average, with the other very connected neurons [21–23]. This

* Corresponding author.
E-mail address: viana@fisica.ufpr.br (R.L. Viana).

https://doi.org/10.1016/j.chaos.2020.110395
0960-0779/

connection architecture is consistent with the fact that the neuronal network increases in size by the addition of new connections, and the last one, preferentially connects to a well connected neuron [11,24,25].

The local neuron dynamics can be described by a large number of mathematical models. One of most important, both physiologically and historically, are the Hodgkin-Huxley [28] equations. When large assemblies of Hodgkin-Huxley neurons are considered, the number of coupled differential equations can be often a problem for computer simulations. In this sense, sometimes it is better to use simpler models, which still retain some relevant aspects of the dynamics one has to consider.

This is the case, for example, of bursting neurons. While the Hodkgin-Huxley equations can be modified to include a slow calcium dynamics enabling us to describe bursting neurons [29], the resulting equations are relatively complicated to use in networks with a large number of neurons. If one is focusing on dynamical issues related to bursting dynamics, as it is in the present work, it would be justifiable to use simpler models, provided they keep some of the dynamical features to be considered. In our work we choose to describe neuron bursting dynamics by a discrete-time two-dimensional map proposed by Rulkov [30].

Assemblies of coupled Rulkov neurons have been shown to synchronize their bursting rhythms, depending on the strength of the coupling term. The presence of synchronized neuronal rhythms has been related to a number of pathologies such as Parkinson's disease, epilepsy and essential tremors [31–34]. One way to suppress neuronal synchronization is to apply electrical stimulus to specific targets in the brain, using a number of techniques collectively called *deep brain stimulation* [35,36]. The effectiveness of those techniques to mitigate pathological rhythms is a strong motivation for developing theoretical approaches that can suggest improved ways to apply external stimuli which suppress synchronization at a minimal cost [37–40].

The main goal of the present work is to investigate numerically the usefulness of a method for suppression of bursting synchronization through a feedback control technique, applying a signal in our neuronal network whose intensity depends on the time-delayed mean field. From the network point of view we can consider the brain as a clustered network, which is a network formed by interacting sub-networks [4]. In this case, the clusters are the sub-networks themselves, and neurons in a given sub-network can be connected with other neurons in the same or a different cluster [5,6]. Perhaps the simplest mathematical model in this sense would be a network of networks, with two levels of description: in the first level, each sub-network is a cluster of neurons linked by electric and chemical synapses. In the second level, each sub-network is a node of another network, where the connections are now of anatomical or functional type. For example, we can model the first level using small-world networks of individual networks and the second level using randomly chosen connections among individual neurons [42].

In the present work we use a scale-free connection architecture to the sub-networks and, for the second level, a human connectivity matrix, obtained experimentally by Lo and collaborators using MRI and tractrography techniques [41]. In the first level each network is generated according to Barabási-Albert procedure [43,44]. The second level connects 78 scale-free sub-networks through a healthy human connectivity matrix and a neuronal activation function. The normalization of the coupling term depends on the amount of incoming and outgoing connections of the neurons that constitute the network. Since bursting synchronization is an expected effect for the coupled neurons we use an external time-delayed feedback signal and verify in what extent we suppress totally or partially synchronization.

This article is organized as follows: in Section 2, we introduce the procedure to construct the network of scale-free networks, the mathematical description of the neuron coupling and the discrete-time map used to generate bursting neuronal dynamics. In Section 3, we investigate the synchronization properties of the system using a number of numerical diagnostics: we assign a phase to the bursting dynamics and a suitably defined order parameter to quantify the presence of phase synchronization. Moreover, we introduce the technique used to suppress the neuronal synchronization using an external signal modulated by the time-delayed mean field, and investigate how the control parameters influence the effectiveness of the synchronization suppression so obtained. The last Section is devoted to our Conclusions.

2. Network model

2.1. Scale-free sub-networks

We consider a network of networks model where each sub-network is a scale-free network generated by the Barabási-Albert procedure. In the scale-free model new nodes tend to connect to the node that already has most connections. This construction mechanism gives the network two important characteristics: growth and preferential attachments, the latter being what gives rise to hubs, which are the most connected nodes of the network [16].

The Barabási-Albert procedure, for the growth of a scale-free network, can be described as follow: initially the network begins with one node, and, at each step of time a new node is added in the network according to the probability $\Gamma(k_i) = k_i / \sum_j k_j$. We construct 78 sub-networks, each of them with 200 nodes, according to this rule and set that each neuron must have at least two connections (incoming and outgoing). The scale-free networks are characterized by a degree probability distribution that follows a power-law $P(k) \propto k^{-\gamma}$, where $P(k)dk$ gives the probability of finding a node with degree between k and $k + dk$[7,16]. In general for a scale-free network $2.0 < \gamma < 3.0$.

Fig. 1 (a)–(c) show numerical approximations to this distribution, with power-law fits with maximum (blue) and minimum (magenta) values for the power-law exponents. In Fig. 1(a) we present the distribution for all conections, with exponents $\gamma = 2.99$ (maximum) and minimum value is $\gamma = 2.02$ (minimum). The probability distribution of degrees for incoming connections have exponents $\gamma = 2.75$ and $\gamma = 2.00$ [Fig. 1(b)]. For the outgoing connections, [Fig. 1(c)], the maximum and minimum exponents are $\gamma = 2.91$ and $\gamma = 2.00$, respectively.

The connection is realized through synapses that can be of two types: chemical synapses, which are mediated through the release and absorption of a neurotransmitter; and the electrical synapses, based on the contact between two axonal terminals [26,27]. In this paper we consider chemical synapses only.

2.2. Human connectivity matrix

The human connectivity matrix used in the present model was built from data obtained by Lo and collaborators using Diffusion MRI tractography and automated anatomical labeling [41]. The brain cortex was divided into 78 areas with 39 cortical regions for each hemisphere. A node for this network is defined if there are at least 3 connected fibers assigned to that cortical area, the relative number of fibers describing the weight of each node. Fig. 2 illustrates the weighted connectivity matrix, where the weight of each node is 0 (white), 1 (magenta), 2 (cyan), and 3 (orange), representing no connections (or unknown), sparse, intermediate and dense connections, respectively [47].

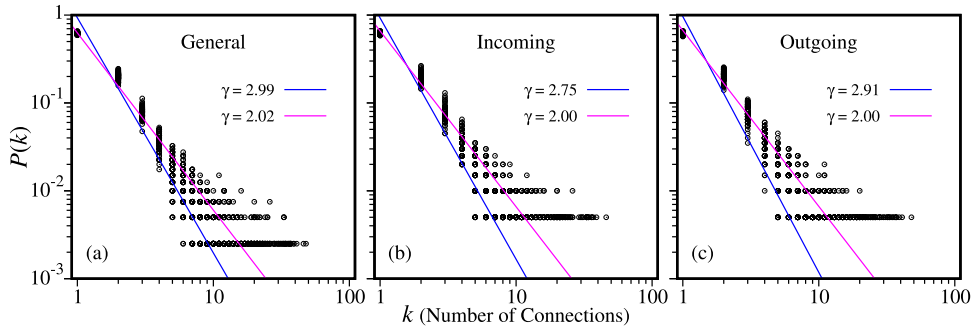

Fig. 1. Connection probability for 78 scale-free networks. The lines are power-law fits for two different values of the power-law exponent. Three cases are considered: (a) all connections, (b) incoming connections, (c) outgoing connections.

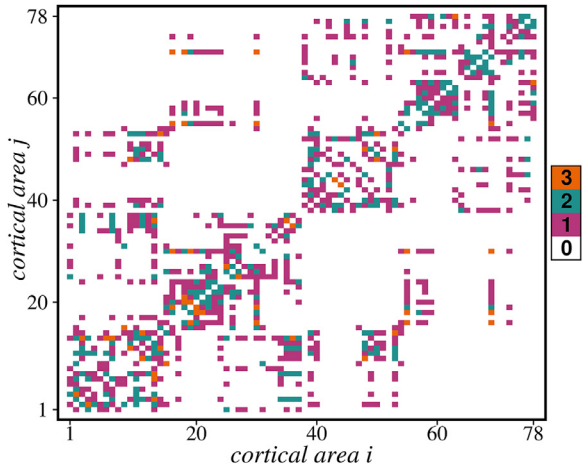

Fig. 2. Connectivity weighted matrix based on data obtained by Lo et al. [41]. The connection weights are indicated by a colorcode.

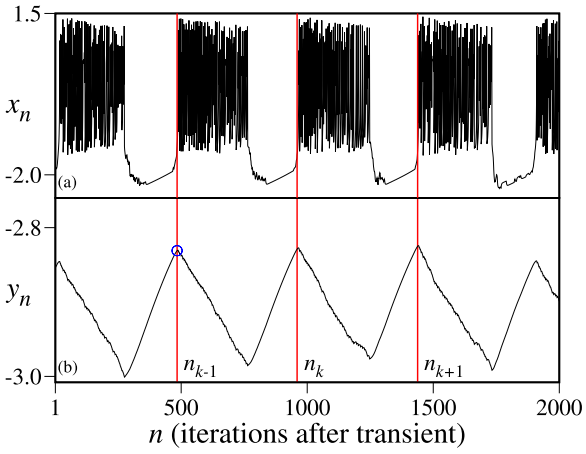

Fig. 3. Time series of the variables (a) x and (b) y for a neuron described by Rulkov's map (1)-(2) for $\alpha = 4.1$, $\sigma = 0.001$, and $\rho = -1.0$. In (b) we indicate the discrete times at which bursting cycles begin. The blue circle indicates a local maximum of the y variable. (For interpretation of the references to colour in this figure legend, the reader is referred to the web version of this article.)

The model implementation in two levels is done as follows. The first level is composed by scale-free sub-networks obtained through the Barabási-Albert procedure. The corresponding adjacency matrix has elements equal to 1 if there is a connection between neurons i and j, and 0 otherwise. In the second level we will use the human connectivity matrix, which describes the connections between different cortical regions, that is, between different sub-networks. The connections between different cortical regions p and d are assigned by the following rule: we randomly choose (with uniform probability) a neuron i from sub-network p and a neuron j from sub-network d, with the same probability. The weights indicated by colors in Fig. 2 represent the number of randomly assigned connections between the cortical regions: the weights 1, 2 or 3 mean 50, 100 or 150 connections between neurons belonging to the cortical areas, respectively [47].

The resulting two-level symmetric connectivity matrix elements are denoted by $W_{(j,d)}^{(i,p)}$ which identifies how a neuron i, in the network p, is connected to a neuron j in the network d. As an example, from Fig. 2, the cortical regions $p = 40$ and $d = 2$ are connected with unity weight (magenta), representing 50 connections among randomly chosen neurons from the scale-free sub-networks corresponding to these cortical regions. Similarly the cortical regions $p = 78$ and $d = 77$ have a connection with weight 2 (cyan), i.e. there are out of 100 connections among neurons from these sub-networks.

2.3. Neuronal bursting dynamics

Since our goal is to investigate bursting synchronization, the neurons belonging to each cortical area must display bursting behavior, even when isolated. Since we are more interested in the dynamics of the coupled network rather than the individual bursting behavior, we can choose a minimal model which exhibits bursting, like the two-dimensional discrete-time map proposed by Rulkov [30]:

$$x_{n+1} = f(x_n, y_n) = \frac{\alpha}{1 + x_n^2} + y_n, \tag{1}$$

$$y_{n+1} = y_n - \sigma(x_n - \rho), \tag{2}$$

where x_n represents the membrane potential and y_n is a recovery variable at discrete time $n = 0, 1, 2, \ldots$, and α, ρ, σ are the parameters of the model.

Different combinations of ρ, σ and α give rise to different of neural firing patterns such as rest, spikes and bursts [30]. We will fix $\sigma = 0.001$, $\rho = -1.0$, and keep α within the interval $[4.1, 4.3]$ so as to have bursting behavior. One example is displayed in Fig. 3(a) and (b), which depict the time evolution of x and y variables, respectively, for $\alpha = 4.1$. The membrane potential presents bursting cycles beginning at local maximum of the y-variable [an example being the blue circle in Fig. 3(b)].

The dynamics of the network of coupled Rulkov neurons is given by

$$x_{n+1}^{(i,p)} = f\left(x_n^{(i,p)}, y_n^{(i,p)}\right) + A_n^{(i,p)}, \tag{3}$$

where $x_n^{i,p}$ and $y_n^{i,p}$ are the variables for a Rulkov neuron attached to the ith node belonging to the pth sub-network, where $i = 1, 2, \ldots, 200$ (for each scale-free sub-network) and $p = 1, 2, \ldots, 78$

(for the human connectivity matrix where each element is a sub-network). The coupling term $A_n^{(i,p)}$ represents the effect of the chemical synapses linking the (i, p) neuron to the rest of the network. Each neuron has at least two connections: one ingoing and other outgoing. There are no electrical synapses in our model, since electrical synapses require neuron membranes to be close enough to allow ion currents, and this would mean local couplings, which are not considered in a scale-free model for the sub-networks.

The expression for the coupling term, taking into account the two-level network structure (human connectivity matrix of scale-free sub-networks), is

$$A_n^{(i,p)} = \frac{\varepsilon}{k^{(i,p)}} \sum_{d=1}^{N} \sum_{j=1}^{M} W_{(j,d)}^{(i,p)} H\left(x_n^{(j,d)} - \theta\right)\left(x_n^{(i,p)} - V_{(j,d)}^{(i,p)}\right), \tag{4}$$

where ε is the coupling strength of the chemical synapses, $N = 78$ and $M = 200$ are the numbers of sub-networks and neurons in each sub-network, respectively.

The connectivity matrix is expressed by $W_{(j,d)}^{(i,p)}$ where j and i represent the neurons, and p and d represent the cortical regions. The neuronal activation function is given by the Heaviside unit-step function $H(x)$, and $\theta = -1.0$ is a threshold which takes on the same values for all neurons. The elements of the connection potential matrix are denoted $V_{(j,d)}^{(i,p)}$, which can be $+1.0$ or -0.5 if the chemical synapse is excitatory or inhibitory, respectively. We suppose that chemical synapses are 25% inhibitory and 75% excitatory [48], and the values of $V_{(j,d)}^{(i,p)}$ are randomly chosen according to this rule. The coupling term is normalized by the number of connections, given by

$$k^{(i,p)} = \sum_{d=1}^{N} \sum_{j=1}^{M} H\left(W_{(j,d)}^{(i,p)}\right). \tag{5}$$

3. Results and discussion

3.1. Bursting synchronization

The bursting activity is periodic and can be described by a geometric phase which increases by 2π at each bursting cycle. As shown in Fig. 3(b), the beginning of each cycle occurs at a local maximum of the variable y, and we denote by n_k the instant of time at which the kth burst starts [see Fig. 3(b)]. If we consider that the difference between n_k and n_{k+1} is the time when the next cycle of bursts starts, we can define a phase that grows 2π as $n_k \leq n \leq n_{k+1}$ [53] as

$$\varphi_n = 2\pi k + 2\pi \frac{n - n_k}{n_{k+1} - n_k}. \tag{6}$$

There is bursting synchronization if two or more neurons start their bursting cycles approximately at the same time, even when the spiking may be not correlated. Using the above defined bursting phase this means that the phases are equal, up to a given tolerance. For an assembly of bursting neurons, it is convenient to measure the synchronization from the Kuramoto's order parameter magnitude [49–52] at time n

$$R_n = \frac{1}{N_T} \left| \sum_{j=1}^{N_T} \exp\left(i\varphi_n^{(j)}\right) \right|, \tag{7}$$

where $\varphi_n^{(j)}$ is the bursting phase for the jth neuron at time n. The values of R_n are expected to oscillate with time, and have a convergent behavior if we wait a transient time n_0, in such a way that we compute a time average $R_m = 1/(n_1 - n_0) \sum_{n=n_0}^{n_1} R_n$ for n_1 large enough. If the neurons are totally synchronized we have $R_m = 1$ and, if they are completely non-synchronized $R_m = 0$. Partial synchronization is thus characterized by the range $0 < R_m < 1$ [49,51].

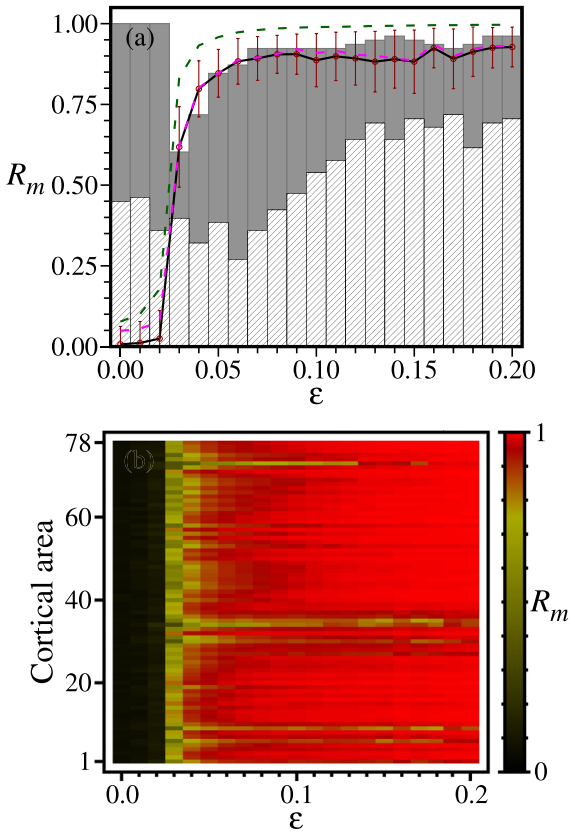

Fig. 4. (a) The dark curves represent the average Kuramoto order parameter as function of the chemical synaptic strength. The dashed curves delimit the maximum (dark-green) and minimum (magenta) values of R_m. The gray vertical bars represent a fraction of the sub-networks that has values of R_m larger than for the overall network. The hatched vertical bars represent the quantity of sub-networks for which R_m is beyond a plus or minus deviation δ, which is indicated by the red bars. (b) Average Kuramoto order parameter (in colorscale) for all 78 cortical areas. (For interpretation of the references to colour in this figure legend, the reader is referred to the web version of this article.)

The definition (7) can be applied to a sub-network, for which $R_m(p)$ denotes the mean order parameter magnitude for the pth cortical area, and j runs from 1 to $N_T = 200$. If it is applied to the network as a whole, then $N_T = NM = 78 \times 200$. Fig. 4(a) displays the variation of the order parameter magnitude of the entire network R_m as a function of the coupling coefficient ε. We used $n_0 = 10^5$ and $n_1 - n_0 = 2 \times 10^3$. Since the initial conditions for the neurons are randomly chosen we have repeated each computation for 4 sets of distinct initial conditions $\left(x_0^{(i,p)}, y_0^{(i,p)}\right)$. There is an abrupt growth in the value of R_m occurring for a value of ε inside the interval (0.02,0.03), after which R_m has small fluctuations near its maximum value of about 0.8. Accordingly we also computed the mean order parameter magnitude for each sub-network. Since there are too many of them to show, it suffices to exhibit the maximum and minimum values of R_m for each value of ε. This is indicated in Fig. 4(a) by dashed curves for the minimum (magenta) and maximum (dark-green) values of the order parameter, respectively, calculated for the individual sub-networks, provided they have a greater value of R_m than for the overall network. Hence the magenta dashed curve is expected to be close to the dark curve for the whole network, what is indeed observed in Fig. 4(a).

The quantity of sub-networks whose Kuramoto order parameter is between the dashed lines is also represented in Fig. 4(a) as a fraction of the total sub-networks by gray vertical bars for each value of ε. A significant fraction of the subnetworks presents

greater synchronization than the composition of all of them. For values of $\varepsilon < 0.02$, all sub-networks are more synchronized than the overall network. Similarly, for $\varepsilon > 0.06$, more than 90% of the sub-networks presents this feature, indicating that the sub-networks are internally synchronized, but are not synchronized with each other. The hatched vertical bars represent the quantity of sub-networks whose values of R_m are beyond a plus or minus deviation given by

$$\delta = \sqrt{\frac{1}{M}\sum_{i=1}^{M}\left(R_m - R_m^{(i)}\right)^2} \tag{8}$$

and are represented in Fig. 4(a) by error bars for the black curve of the entire network R_m. Comparing these error bars with the hatched vertical bars we see that the sub-network order parameter $R_m(p)$ is always less than a deviation from the average order parameter of the network R_m. This deviation illustrates the disparity between the synchronization degrees within each sub-network and the overall network. Large values for deviation are associated with much more or less synchronized sub-networks than the composition of all networks. We emphasize that the order parameter magnitude of the whole network R_m is typically different from the values averaged over the sub-networks $\bar{R} = (1/N)\sum_{p=1}^{N} R_m(p)$.

The differences among the synchronization levels of the various cortical areas can be appreciated in Fig. 4(b), which depicts the average Kuramoto order parameter $R_m(p)$ for all 78 cortical areas as a function of the chemical synaptic strength ε. The threshold of synchronization is $\varepsilon \approx 0.02$ for all cortical areas. On the other hand, if ε is large enough nearly all areas become synchronized. For intermediate values of ε the average Kuramoto order parameter increases as ε grows, reaching different phase synchronization values. On comparing Fig. 4(a) and (b) we can identify those cortical areas that, although internally synchronizes, fail to synchronizes with each other. This is particularly true for a number of cortical areas between 1 and 10, 30 and 40, 70 and 78. They are just those highly connected cortical areas shown in the connectivity matrix of Fig. 2.

3.2. Suppression of bursting synchronization

As we commented in the Introduction, bursting synchronization may not be a desirable behavior for the network, since neuronal synchronization has been related with a number of diseases like Parkinson, epilepsy, and essential tremor. Hence, once we know that the network as a whole or its sub-networks are synchronized, we are interested to investigate ways to mitigate or even suppress synchronization. Many techniques have been proposed to accomplish this task, collectively called *deep brain stimulation*. One of these techniques consists in applying an external electric signal to the parts of the brain, what would imply in a time-dependent term added to the membrane potential x in Eq. (3) for the coupled Rulkov neurons.

If this signal is a simple harmonic function of the form $B\sin(\omega n)$, where B and ω are the amplitude and frequency, respectively, this procedure has been shown to diminish bursting synchronization levels. However the usefulness of this function is limited by the large amplitudes needed and/or the large number of neurons that have to be excited to produce such effect. An alternative procedure consists in monitoring the mean field and adjusting the signal amplitude to the desired effect, what also includes a time delay due to the need of computing in real time the mean field. This can be included by means of a delayed feedback signal $\mathscr{F}_n(p,\tau)$, to be applied to the cortical region p with a delay time τ[54,55]. Thus, the mean field is incorporated to the fast variable Rulkov's map:

$$x_{n+1}^{(i,p)} = f\left(x_n^{(i,p)}, y_n^{(i,p)}\right) + A_n^{(i,p)} + \varepsilon_F\,\mathscr{F}_n(p,\tau), \tag{9}$$

where ε_F is the feedback signal intensity and τ is the time delay. The delayed mean field term for the cortical region p is the network average of the membrane potential for each neuron therein

$$\mathscr{F}_n(p,\tau) = \frac{1}{M}\sum_{i=1}^{M} x_{n-\tau}^{(i,p)}. \tag{10}$$

If the (uncontrolled) sub-network p is synchronized at a given time n, the current mean field $\mathscr{F}_n(p,\tau=0)$ is nearly equal to the evolution of x_n for each neuron, which is characterized by a large oscillation in the amplitude and with a relatively large variance $\mathrm{Var}(\mathscr{F}_n(p,\tau=0))$. On the contrary, if the sub-network is completely non-synchronized the mean field will have a low amplitude fluctuation around zero, that is a low variance. Since the goal of the control procedure is to reduce the synchronization level, we expect that on applying the control term with amplitude ε_F, the variance of the mean field with control should be the smallest possible. Pikovsky and Rosenblum proposed the following synchronization suppression factor [56],

$$S = \sqrt{\frac{\mathrm{Var}(\mathscr{F}_n(p,\tau=0))}{\mathrm{Var}(\mathscr{F}_n(p,\tau))}}. \tag{11}$$

where $\mathrm{Var}(\mathscr{F}_n(p,\tau=0))$ and $\mathrm{Var}(\mathscr{F}_n(p,\tau))$ are the mean field variances without and with the feedback signal input, respectively. Since $\mathrm{Var}(\mathscr{F}_n(p,\tau=0)) \neq 0$ an efficient suppression of synchronization is characterized by $S > 1$, i.e., the higher S is, the better is the suppression effect. Conversely a value $0 < S < 1$ would imply reinforcement of the synchronization, an effect clearly undesirable.

Using our network model the time-delayed feedback control signal (9) was applied on a certain number of randomly chosen cortical areas, for four different proportions of cortical areas, starting at 25% until reaching 100% of the areas, as illustrated in Fig. 5. The actual number of cortical regions to which the control was applied has been rounded up. The left panels of Fig. 5 show the suppression coefficient S (actually its natural logarithm in a colorscale) as a function of the control amplitude ε_F and time delay τ, whereas the right panels show curves of S as a function of ε_F for different values of τ.

The log-colorscale for S is convenient since it is a heat-map: blue regions are cases for which the suppression reaches satisfactory values and red regions correspond to reinforcement of synchronization, which is undesirable. When the control term is applied to 25% of the cortical regions all regions of the control parameter plane yield good suppression of synchronization [Fig. 5(a)], S reaching a maximum value of 2.58 for time-delay $\tau = 160$ [Fig. 5(b)]. In this way the region that presents the high values for suppression is between $\tau = 140$ and 180 and ε_F between 0.20 and 0.30.

When 50% of the cortical regions are controlled, we notice the presence of a small region in red that indicates that the method has a result in opposite to what we want, i.e, the region in red shows where the synchronization is not suppressed but stimulated by the application of feedback technique [Fig. 5(c)]. However the regions for which the control is efficient agains synchronization yield values of S higher than 3.0 for time-delay 140 (measured in units of discrete time used in the map) [Fig. 5(d)]. The best values of suppression in this case lie in the intervals $\tau = 120$ to 160.

When we increase the percentage of cortical regions disturbed by feedback to 75%, the suppression method begins to present much larger synchronization stimulus regions than for the 25% and 50% cases [Fig. 5(e)-(f)]. Finally when we disturb 100% of the cortical regions it is clearly visible that the undesirable cases take over of almost every parameter space [Fig. 5(g)-(h)]. Nevertheless the best values of suppression for 75% and 100% of control regions are from $\tau = 100$ to 140 and from $\tau = 180$ to 200, respectively.

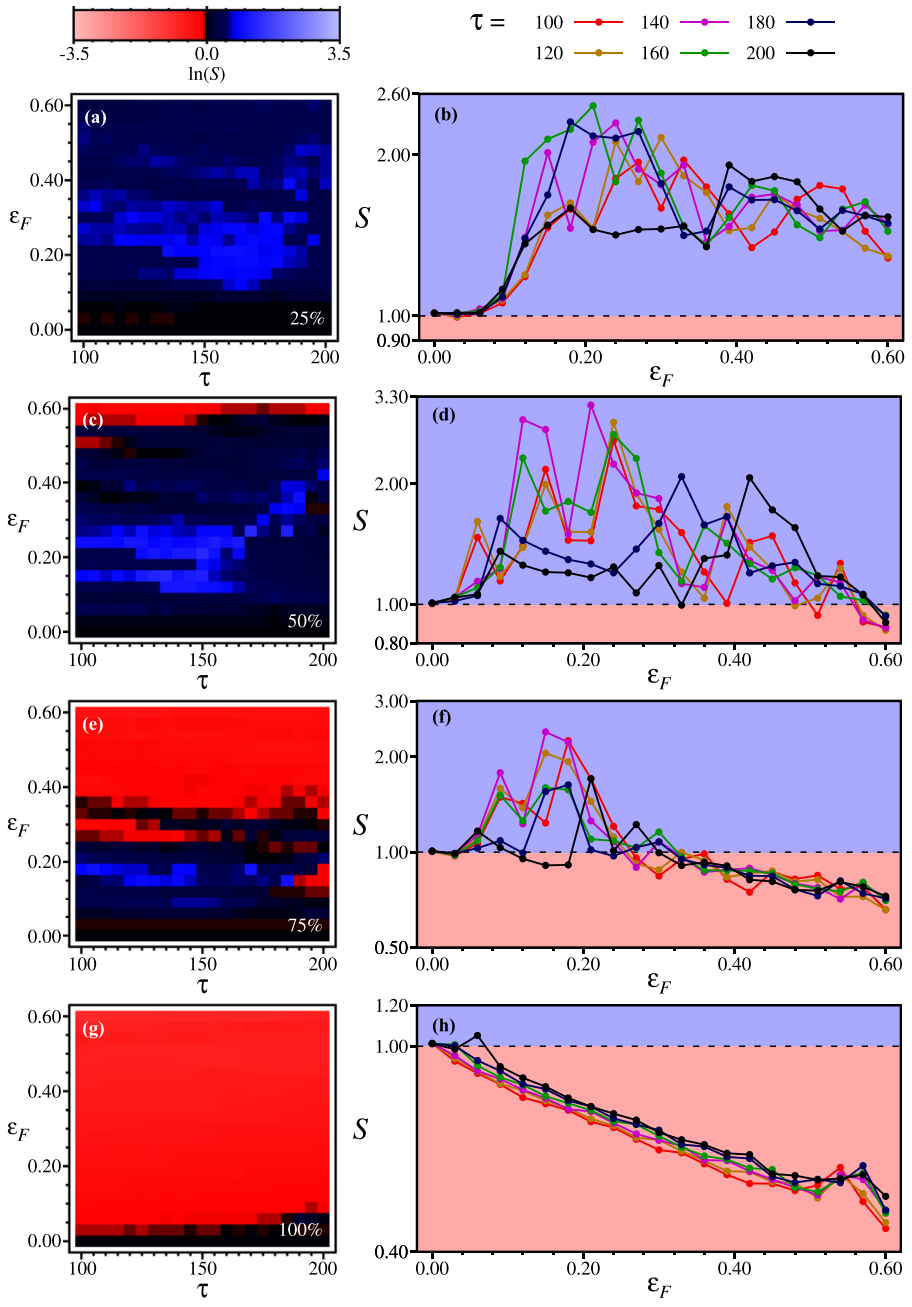

Fig. 5. Synchronization suppression factor (in log-colorscale) as a function of the control amplitude ε_F and time-delay τ when the control is applied to (a) 25%,(c) 50%,(e) 75%, and (f) 100% of the cortical areas in the human connectivity matrix and chemical coupling strength $\varepsilon = 0.2$. The corresponding variation of S with ε_F and various values of τ is depicted in (b), (d), (f), and (h). Values of $S > 1$ correspond to synchronization suppression.

As dealing with a scale-free model we have the presence of hubs in ours networks. Hubs are formed due to the preferential attachment characteristics in the growth of a scale-free network and have the highest degree of each sub-network. In a hypothetical experiment for deep brain stimulation a probe used to inject an electric signal would be placed in a certain place of a cortical area. If by chance this probe is applied to a neuron hub, we will have a different effect in comparison with other, low-connected neurons belonging to a given cortical area.

The efficiency of synchronization suppression we observed due to the external time-delayed control signal displays qualitatively similar features if we changed the networks in each cortical area from scale-free to a random (Erdös-Renyi) [13] and a small-world network [15]. As the percentage of perturbed cortical areas is increased this similarity is even greater. Moreover, instead of the human connectivity matrix we repeated our numerical simulations using the cat cerebral cortex matrix, with information from the neuroanatomical tract-tracing experiments collected and organized by Scannell and coworkers [45,46,57]. In this matrix the cat cerebral cortex has been divided into 65 cortical areas, interconnected by fibers of axons [19].

We also used another dataset from the PIT Bioinformatics Group data available at https://braingraph.org/cms/human/ in addition to Lo's data [58]. The connectomes were generated from MRI scans obtained from the Human Connectome Project [59–61]. They have computed structural connectomes of 426 human subjects in five different resolutions of 83, 129, 234, 463, and 1015 nodes and several edge weights. We choose the matrix that has 83 cortical

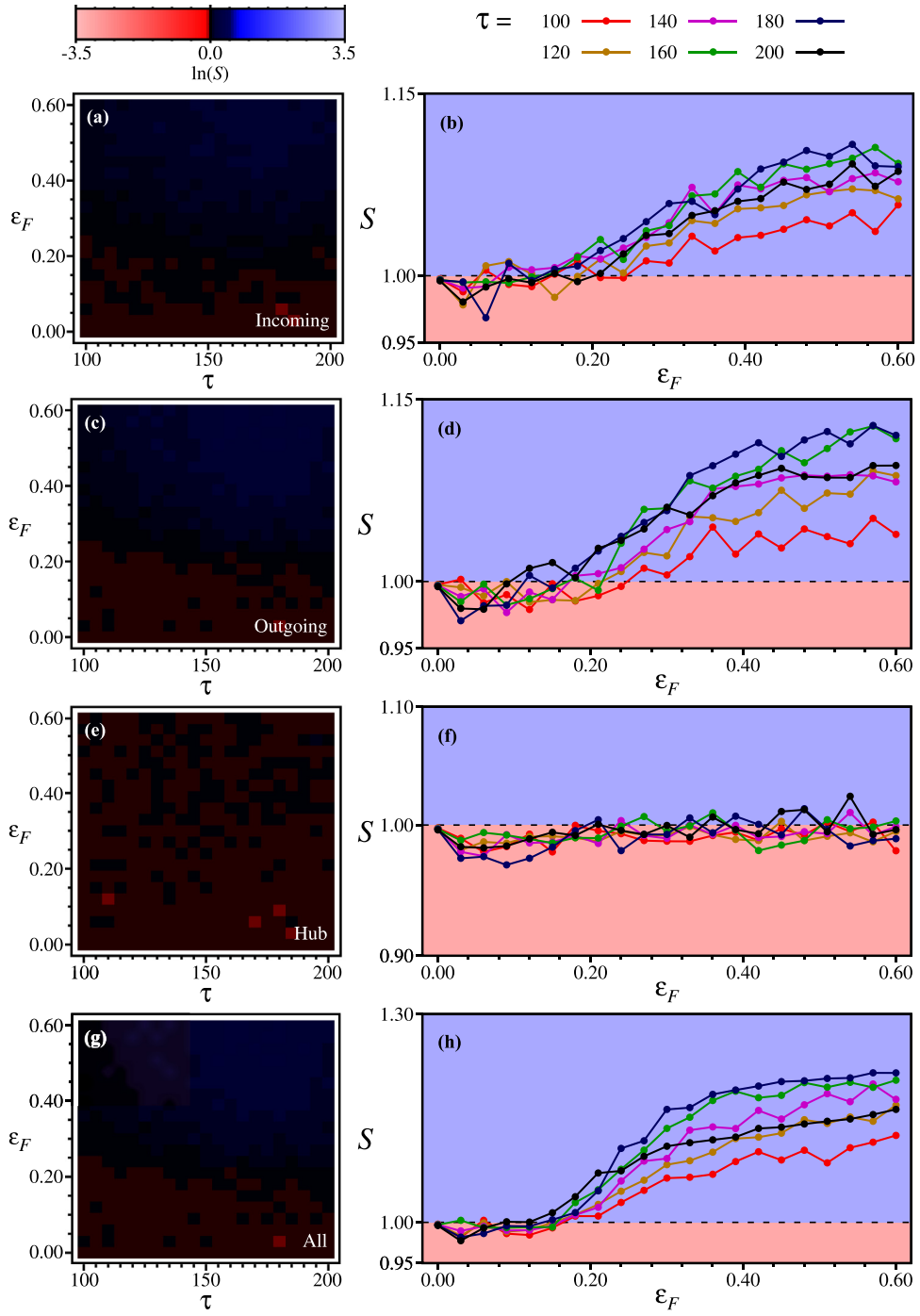

Fig. 6. Synchronization suppression factor (in log-colorscale) as a function of the control amplitude ε_F and time-delay τ when the control is applied to 100% of the cortical areas in the human connectivity matrix and chemical coupling strength $\varepsilon = 0.2$. The control was applied to neuron hubs only (a), neurons with incoming (b) and outcoming (c) connections, and the whole network (d). The corresponding variation of S with ε_F and various values of τ is depicted in (b), (d), (f), and (h). Values of $S > 1$ correspond to synchronization suppression.

regions and 1064 brains. Among these 1064 brains, we chose 20 of them. Quantitatively, the results are not the same as Lo's data, but qualitatively they indicate similar results, suggesting that our results are not limited to a specific network model or database.

In scale-free networks we can devise three different ways of applying the time-delayed feedback signal: we can either apply the signal to a single neuron hub, or the nodes with incoming and outgoing connections. The sum of these three contributions gives the total number of neurons in the network. Accordingly, the left panels in Fig. 6 represent (in a log-colorscale) the suppression coefficient S as a function of the signal amplitude ε_F and time delay τ; and the right panels show plots of S against ε_F for some selected values of τ.

When we apply the control on the hubs only (one for each cortical area) we have a quite poor performance since the values of S are either less than unity of with slightly higher values [Figs. 6(a)-(b)], even when ε_F is as large as 0.50. Better results are obtained when the control is applied to all neurons with incoming connections [Fig. 6(c)-(d)], specially if $\varepsilon_F > 0.20$. A similar situation occurs if the control is applied to neurons with outgoing connections

[Fig. 6(e)-(f)]. The effect of applying the control on all neurons of the network is illustrated by Fig. 6(g)-(h). There results that the hubs, although better connected than the remaining neurons in a sub-network, yield an effect that is much weaker than the totality of the neurons are considered. Hence, strictly from the control point of view, the scale-free architecture does not play a pivotal role.

4. Conclusions

In this paper we present results of numerical simulations of a network of networks model with scale-free properties for the human cerebral cortex, through chemical couplings considering as local dynamics the Rulkov map. The model was built so that the connections between the cortical regions are given by an experimentally obtained connectivity matrix and the connections within a cortical area were obtained from the Barabasi-Albert procedure. Individual Rulkov neurons are set to exhibit bursting behavior and we focus on bursting synchronization and possible ways to partial or total suppression of synchronized behavior, having in mind potential applications for the mitigation of pathological rhythms.

Model parameters were chosen so as to ensure bursting synchronization of the network. If the strength of chemical synapses is relatively small there is no synchronization at all, and after a threshold the neurons of different cortical areas become increasingly synchronized but the cortical areas themselves are not mutually synchronized. This could be regarded as a situation more realistic, since pathological rhythms have been related to synchronized behavior of small parts of the brain. It is only for sufficiently large values of the coupling strength that the network becomes synchronized as a whole. A macrosynchronization of this kind is not likely to occur in practice, though, what suggests a limit for the values of the chemical synapse strength within the context of this model.

The control of synchronized behavior was modelled using a time-delayed feedback signal, which takes into account the local mean field. We address the question of how to choose parameters that yield the best performance with regard to the suppression of synchronization. Our main result is that the efficiency of suppression actually decreases with the percentage of the cortical areas subjected to the external control. In fact, the mechanism of suppression of synchronization is to induce neurons to desynchronize their individual behaviors due to a relatively weak external perturbation. However, if the latter is too strong, as it is the case when many cortical areas are controlled, *the neurons start synchronizing with the external signal* and the net result is a reinforcement of the effect which we wish to suppress.

Another result of our numerical investigation is that the internal scale-free structure of cortical areas, characterized by the presence of highly connected neuron hubs, does not play a key role in the suppression of synchronization. Since in an artificial neuronal network we know in advance what are the hubs for each cortical area, we were able to compare a control applied on the hubs with those applied to the rest of the network, showing that a hypothetical choice of hubs does not yield significative results for the synchronization suppression.

As a concluding remark, we have applied the same control technique to similar neuronal network models for which the lower level networks have also random and small-world networks, and the higher level connectivity matrix is taken from data obtained for other human and mammals neuronal connection matrices. In all these numerical simulations we obtained results with qualitatively similar features, suggesting that our results are not limited to the particular network model used in the present work.

Declaration of Competing Interest

The authors declare that they have no known competing financial interests or personal relationships that could have appeared to influence the work reported in this paper.

CRediT authorship contribution statement

Adriane S. Reis: Conceptualization, Data curation, Formal analysis, Investigation, Methodology, Resources, Software, Supervision, Validation, Visualization, Writing - original draft, Writing - review & editing. **Kelly C. Iarosz:** Data curation, Investigation, Methodology, Validation, Visualization, Writing - review & editing. **Fabiano A.S. Ferrari:** Data curation, Investigation, Methodology, Validation, Visualization, Writing - review & editing. **Iberê L. Caldas:** Data curation, Investigation, Methodology, Validation, Visualization, Writing - review & editing. **Antonio M. Batista:** Data curation, Investigation, Methodology, Validation, Visualization, Writing - review & editing. **Ricardo L. Viana:** Conceptualization, Funding acquisition, Methodology, Project administration, Resources, Supervision, Validation, Visualization, Writing - original draft, Writing - review & editing.

Acknowledgments

This study was possible by partial financial support from the following agencies: Brazilian National Council for Scientific and Technological Development (CNPq), Coordination for the Improvement of Higher Education Personnel (CAPES), and São Paulo Research Foundation (FAPESP) process numbers 2018/03211-6. The authors are also thankful to MSc. Eduardo L Brugnago for the help given in the treatment of some images and for the constructive discussions.

References

[1] Buzsaki G. Rhythms of the Brain. Oxford University Press; 2006. ISBN:9780195301069
[2] Hilgetag CC, Kaiser M, Graben PB, Zhou C, Thiel M, Kurths J. Lectures in Supercomputational Neuroscience (Dynamics in Complex Brain Networks). Springer; 2008. ISBN:9783540731597
[3] Zamora-López G, Zhou C, Kurths J. Exploring brain function from anatomical connectivity. Front Neurosci 2011;5:83.
[4] Zamora-López G, Zhou C, Kurths J. Graph analysis of cortical networks reveals complex anatomical communication substrate. Chaos 2009;19:015117.
[5] Zhao M, Zhou C, Liu J, Lai CH. Competition between intra-community and inter-community synchronization and relevance in brain cortical networks. Phys Rev E 2011;84:016109.
[6] Wang S-J, Hilgetag CC, Zhou CS. Sustained activity in hierarchical modular neural networks: self-organized criticality and oscillations. Front Comput Neurosci 2011;5:30.
[7] Barabási A-L. Linked: How everything is connected to everything else and what it means. Plume 2003. ISBN: 0452284392
[8] Dorogovtsev S, Mendes JF. Evolution of networks. Adv Phys 2002:1079–187.
[9] Milgram S. The small-world problem. Psychol Today 1967:61–7.
[10] Travers J, Milgram S. An experimental study of the small world problem. Sociometry 1969:425–43.
[11] Estrada E. The structure of complex networks. New York: Oxford University Press; 2011.
[12] Strogratz S. Exploring complex networks. Nature 2001;410:268–76.
[13] Erdös P, Rényi A. On random graphs i. Publicationes Math 1959;6:290–7.
[14] Bollobás B. Random Graphs. Cambridge University Press; 2001. ISBN 0-521-79722-5
[15] Watts DJ, Strogatz SH. Collective dynamics of 'small-world' networks. Nature 1998;393(6684):440–2.
[16] Barabási A-L, Albert R. Emergence of scaling in random networks. Science 1999;286:507–12.
[17] Sporns O, Zwi JD. The small world of the cerebral cortex. Neuroinformatics 2004;2:145–62.
[18] Bassett DS, Bullmore E. Small world brain networks. Neuroscientist 2006;12:512–23.
[19] Coninck JCP, Ferrari FAS, Reis AS, Iarosz KC, Caldas IL, Batista AM, Viana RL. Network properties of healthy and Alzheimer brains. Physica A 2020;547:124475.
[20] Albert R. Scale-free networks in cell biology. J Cell Sci 2005:4947–57.
[21] Chialvo DR. Critical brain networks. Physica A 2004;32004:756–65.

[22] Sporns O, Chialvo DR, Kaiser M, Hilgetag CC. Organization, development and function of complex brain networks. Trends Cogn Sci 2004;8:418–25.
[23] Equiluz VM, Chialvo DR, Cecchi GA, Buliki M, Apkarian AV. Scale-free brain functional networks. Phys Rev Lett 2005;94(018102):1–4.
[24] Boccaletti S, Latora V, Moreno Y, Chavez M, Hwang DU. Complex networks: structure and dynamics. Phys Rep 2006;424(4):175–308.
[25] Newman MEJ. The structure and function of complex networks. SIAM Rev 2003;45(2):167–256.
[26] Guyton AC, Hall JE. Guyton and Hall textbook of medical physiology. Philadelphia: Elsevier; 2011. ISBN: 1455755699
[27] Siegel GJ, Agranoff BW, Albers RW, Fisher SK, Uhler MD. Basic Neurochemistry: Molecular, Cellular, and Medical Aspects. Raven Press; 1999. ISBN:9780881673432
[28] Hodgkin AL, Huxley AF. A quantitative description of membrane current and its application to conduction and excitation in nerve. J Physiol 1952;117(4):500–44.
[29] Shorten PR, Wall DJN. A Hodgkin-Huxley model exhibiting bursting oscillations. Bull Math Biol 2000;62:695–715.
[30] Rulkov NF. Regularization of synchronized chaotic bursts. Phys Rev Lett 2001;86(1):183–6.
[31] Beutter A, Titcombe MS, Richer F, Gross C, Guehl D. Effect of deep brain stimulation on amplitude and frequency characteristics of rest tremor in Parkinson's disease. Thalamus Rel Syst 2001:203–11.
[32] Jiruska P, Curtis M, Jefferys JGR, Schevon CA, Schiff SJ, Schindler K. Synchronization and desynchronization in epilepsy: controversies and hypotheses. J Physiol 2013;591(4):787–97.
[33] Schnitzler A, Munks C, Butz M, Timmermann L, Gross J. Synchronized brain network associated with essential tremor as revealed by magnetoencephalography. Mov Disord 2009;24:1629–35.
[34] Benito-León J, Serrano JI, Louis ED, et al. Essential tremor severity and anatomical changes in brain areas controlling movement sequencing. Ann Clin Transl Neurol 2018;6(1):83–97.
[35] Morten LK, Ned J, Sarah LFO, Tipu ZA. Translational principles of deep brain stimulation. Nat Rev Neurosci 2007:623–35.
[36] Deep-Brain Stimulation for Parkinsons Disease Study Group, et al. Pathological synchronization in Parkinson's disease: networks, models and treatments. N Engl J Med 2001;345(13):956–63.
[37] Batista CAS, Lopes SR, Viana RL, Batista AM. Delayed feedback control of bursting synchronization in a scale-free network. Neural Netw 2010:114–24.
[38] Lameu EL, Batista CAS, Batista AM, Iarosz K, Viana RL, Lopes SR, Kurths J. Suppression of bursting synchronization in clustered scale-free ("rich-club") neuronal networks. Chaos 2012:043149.
[39] Protachevicz PR, Borges RR, Borges FS, Iarosz KC, Caldas IL, Lameu EL, et al. Synchronous behaviour in cortico-cortical connection network of the human brain. Physiol Meas 2018:074006.
[40] Mugnaine M, Reis AS, Borges FS, Borges RR, Ferrari FAS, Iarosz KC, et al. Delayed feedback control of phase synchronization in a neuronal network model. Eur Phys J – Spec Top 2018;227:1151–60.
[41] Lo C-Y, Wang P-N, Chou K-H, Wang J, He Y, Lin C-P. Diffusion tensor tractography reveals abnormal topological organization in structural cortical networks in Alzheimer's disease. J Neurosci 2010;30(50):16876–85.
[42] Batista CAS, Lameu EL, Batista AM, Lopes SR, Pereira T, Zamora-López G, Kurths J, Viana RL. Phase synchronization of bursting neurons in clustered small-world networks. Phys Rev E 2012;86:016211.
[43] Batista CAS, Batista AM, Pontes JCA, Viana RL, Lopes SR. Chaotic phase synchronization in scale-free networks of bursting neurons. Phys Rev E 2007;76(1):016218.
[44] Batista CAS, Batista AM, Pontes JCA, Lopes SR, Viana RL. Bursting synchronization in scale-free networks. Chaos Solitons Fractals 2009;41(5):2220–5.
[45] Scannell JW, Young MP. The connectional organization of neural systems in the cat cerebral cortex. Curr Biol 1993;3:191.
[46] Scannell JW, Blakemore C, Young MP. Analysis of connectivity in the cat cerebral cortex. J Neurosci 1995;15:1463.
[47] Ferrari FAS, Viana RL, Reis AS, Iarosz KC, Caldas IL, Batista AM. A network of networks model to study phase synchronization using structural connection matrix of human brain. Physica A 2018;496:162–70.
[48] Lee TW. Network balance and its relevance to affective disorders: dialetic neuroscience. New York: Pronoun; 2016.
[49] Kuramoto Y. Chemical oscillations, waves, and turbulence. 8th ed. Berlin: Springer-Verlag; 1984.
[50] Kuramoto Y. Self-entrainment of a population of coupled non-linear oscillators. Lect Notes Phys 1975;39:420–2.
[51] Arenas A, Díaz-Guilera A, Kurths J, Moreno Y, Zhou C. Synchronization in complex networks. Phys Rep 2008;469(3):93–153.
[52] Strogatz SH. From kuramoto to crawford: exploring the onset of synchronization in populations of coupled oscillators. Physica D 2000;143(1):1–20.
[53] Ivanchenko MV, Osipov GV, Shalfeev VD, Kurths J. Phase synchronization in ensembles of bursting oscillators. Phys Rev Lett 2004;93(13):134101.
[54] Rosenblum M, Pikovsky A. Delayed feedback control of collective synchrony: an approach to suppression of pathological brain rhythms. Phys Rev E 2004;70:041904.
[55] Batista CAS, Lopes SR, Viana RL, Batista AM. Delayed feedback control of bursting synchronization in a scale-free neuronal network. Neural Netw 2010;23(1):114–24.
[56] Rosenblum M, Pikovsky A. Controlling synchronization in an ensemble of globally coupled oscillators. Phys Rev Lett 2004;92:114102.
[57] Scannell JW, Burns GAPC, Hilgetag CC, O'Neil MA, Young MP. The connectional organization of the cortico-thalamic system of the cat. Cerebral Cortex 1999;9(3):277–99.
[58] Braingrapg.org. the network of the brain. https://braingraph.org/cms/;2020 [accessed on September 25,2020].
[59] Kerepesi C, Szalkai B, Varga B, Grolmusz G. The braingraph.org database of high resolution structural connectomes and the brain graph tools. Cogn Neurodyn 2017;11(5):483–6. doi:10.1007/s11571-017-9445-1.
[60] Szalkai B, Kerepesi C, Varga B, Grolmusz V. High-resolution directed human connectomes and the consensus connectome dynamics. PLoS ONE 2019;14(4):e0215473. doi:10.1371/journal.pone.0215473.
[61] Kerepesi C, Szalkai B, Varga B, Grolmusz V. How to direct the edges of the connectomes: dynamics of the consensus connectomes and the development of the connections in the human brain. PLoS ONE 2016;206(11(6)):e0158680. doi:10.1371/journal.pone.0158680.